HAL
open science

# PRECURSORS OF CORE-COLLAPSE SUPERNOVAE AND LONG-SOFT GAMMA-RAY BURSTS: PREDICTIONS OF STELLAR EVOLUTION

F. Martins

▶ **To cite this version:**

F. Martins. PRECURSORS OF CORE-COLLAPSE SUPERNOVAE AND LONG-SOFT GAMMA-RAY BURSTS: PREDICTIONS OF STELLAR EVOLUTION. Journées 2018 de la Société Française d'Astronomie & d'Astrophysique, Jul 2018, Bordeaux, France. pp.327-332. hal-01993797

**HAL Id: hal-01993797**

**https://hal.science/hal-01993797v1**

Submitted on 8 Feb 2019

**HAL** is a multi-disciplinary open access archive for the deposit and dissemination of scientific research documents, whether they are published or not. The documents may come from teaching and research institutions in France or abroad, or from public or private research centers.

L'archive ouverte pluridisciplinaire **HAL**, est destinée au dépôt et à la diffusion de documents scientifiques de niveau recherche, publiés ou non, émanant des établissements d'enseignement et de recherche français ou étrangers, des laboratoires publics ou privés.

*SF2A 2018*
*P. Di Matteo, F. Billebaud, F. Herpin, N. Lagarde, J.-B. Marquette, A. Robin, O. Venot (eds)*

# PRECURSORS OF CORE-COLLAPSE SUPERNOVAE AND LONG-SOFT GAMMA-RAY BURSTS: PREDICTIONS OF STELLAR EVOLUTION

F. Martins[1]

**Abstract.** We present a summary of some predictions of stellar evolution regarding the precursors of core-collapse supernovae and long-soft gamma-ray bursts. We describe the effects of rotation, mass loss, metallicity and binarity on the endpoints of stellar evolutionary tracks.

Keywords: Massive stars; core-collapse supernovae; long-soft gamma-ray bursts

## 1 Introduction

Core-collapse supernovae (CC SN) are the final state of evolution of massive stars. They are separated in two categories depending on their spectra: type II SN show hydrogen lines while type Ib and Ic do not. The former are further separated in four sub-categories: Type IIP and IIL and differentiated by the shape of the SN light curve (the former have a plateau, the latter a linear brightness decrease); Type IIn show narrow hydrogen lines, sometimes separated into multiple components; Type IIb first show hydrogen lines that subsequently vanish and are replaced by helium lines. Type Ib and Ic are separated by the presence (respectively absence) of helium lines. Finally the broad line SN (type Ic-BL) have unusually broad lines. They are the only SN associated with long-soft gamma-ray bursts (LGRB). About 75% of CC SN are of type II (type IIP being the most frequent one) and 25% are type Ibc.

The search for progenitors of CC SN relies on the existence of pre-SN images of the environment of the SN explosion site. If a star is identified at the position of the SN, its properties can be inferred from photometry. If no star is identified, an upper limit on the progenitor's luminosity can be placed. This technique has been applied successfully to identify 13 progenitors of type II SN as well as upper limits on the magnitude of 13 additional type II SN (Smartt 2009, 2015). Progenitors of type Ib and Ic SN have been only tentatively identified in two cases: one for a type Ib SN (Cao et al. 2013; Groh et al. 2013a) and one for a type Ic SN (Van Dyk et al. 2018). Fourteen type Ibc SN have upper limits on the brightness of their progenitors Smartt (2015). Once placed on a Hertzsprung-Russell (HR) diagram, almost all progenitors have luminosities below $\log \frac{L}{L_\odot} < 5.1$, which corresponds to initial masses in the range 8-18 $M_\odot$. Besides the two tentative type Ibc progenitor candidates, there is no progenitor with a mass in excess of 20 $M_\odot$, while about 10 would have been expected if the Salpeter initial mass function is populated up to 100 $M_\odot$. This raises the question of the fate of the most massive stars (Smartt 2015; Yoon 2015; Groh 2017; Hirschi et al. 2017).

In the following we describe some physical processes that affect the evolution and fate of massive stars according to stellar evolution calculations.

## 2 Effects of physical processes

### 2.1 Rotation

The effects of rotation on the evolution of massive stars have been amply described by Maeder & Meynet (2000) and Langer (2012). The first effect is a break of spherical symmetry: a rotating star is flattened, its radius being smaller at the pole than at the equator. As a consequence, the surface gravity is smaller at the equator. This is usually followed by a lower effective temperature according to the Von Zeipel theorem (von

[1] LUPM, CNRS & Université de Montpellier, CC072, Place Eugène Bataillon, F-34095 Montpellier Cedex 05

© Société Francaise d'Astronomie et d'Astrophysique (SF2A) 2018

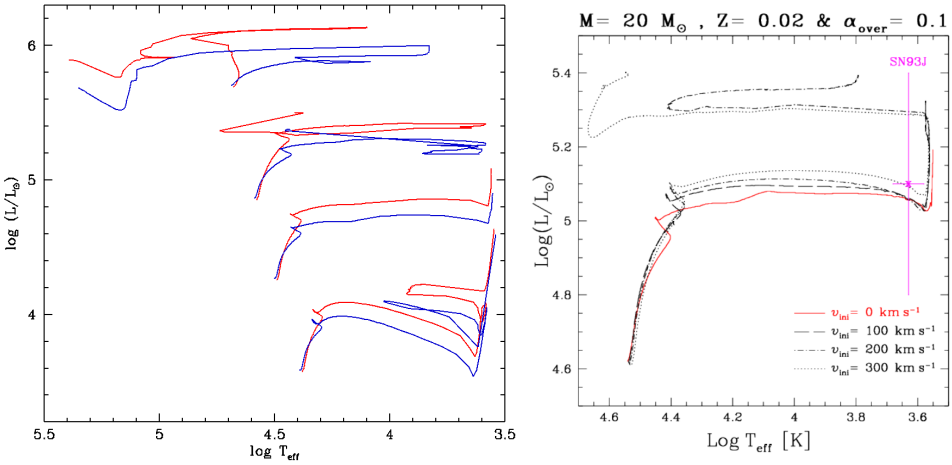


**Fig. 1.** Effect of rotation on evolutionary tracks. **Left:** Evolutionary tracks from Ekström et al. (2012) at solar metallicity. Blue (red) lines correspond to models without (with) rotation. **Right:** 20 $M_\odot$ evolutionary tracks at various rotation velocities, from Hirschi et al. (2017). The pink symbol shows the location of the progenitor of the type II SN 1993J.

Zeipel 1924). This change in the general equilibrium configuration of the star triggers large scale motions and hydrodynamical instabilities in the radiative envelope. These processes lead to a transport of both angular momentum and chemical species. The internal structure of the star is thus different from the non-rotating case. One of the main observational effect is shown in the left panel of Fig. 1 : rotating stars are more luminous (except very close to the zero age main sequence) than non-rotating stars. The reason is the transport of hydrogen-rich material from a region outside the non-rotating convective core, towards the convective core of the rotating star. The resulting extra-helium production increases the mean molecular weight ($\mu$). Since the star's luminosity is proportional to $\mu^3$ (Kippenhahn & Weigert 1994), a rotating star is more luminous. The end point of the evolution is changed (see Fig. 1).

The right panel of Fig. 1 shows the models of Hirschi et al. (2017) for a 20 $M_\odot$ star and various rotational velocities. The end point moves towards higher $T_{\rm eff}$ when rotation increases due to more removal of the external, hydrogen-rich envelope at higher rotation velocity. This is caused by the increased mass loss at higher rotation (Eq. 13 of Maeder & Meynet 2000 - see also next section). As a consequence the endpoint of a 20 $M_\odot$ star can be a red, yellow or blue supergiant depending on the initial rotation velocity.

### *2.2 Mass loss*

Massive stars lose mass at a rate between $10^{-9}$ and $10^{-4}$ $M_\odot yr^{-1}$, sometimes even more in the episodic eruptions associated to the Luminous Blue Variable (LBV) phase. The removal of the star's external layers exposes internal layers to its surface. These internal layers have different chemical compositions and effective temperatures which affect the star's appearance. Mass loss is thus a major ingredient of massive stars evolution (Chiosi & Maeder 1986). Unfortunately, the mass loss rates in the different phases of evolution are largely unknown. For red supergiants (RSG), the wind physics is unknown and the dispersion in the determination of mass loss rates at a given luminosity is extreme (Mauron & Josselin 2011). This leads to large uncertainties in the predictions of stellar evolution.

To estimate the effects of mass loss on the evolution of ∼12-20 $M_\odot$ stars, Georgy (2012) and Meynet et al. (2015) have computed evolutionary tracks with different mass loss prescriptions in the RSG phase. Fig. 2 shows the results of the study of Georgy (2012). When mass loss rates are increased the endpoint of the 15 $M_\odot$ track moves towards the left part of the HR diagram. Said differently, red supergiant progenitors correspond to "low" mass loss rates, while yellow supergiants are obtained for higher mass loss rates. The position of progenitors of type II SN can be reproduces by tuning the rate of mass loss (Fig. 2, right panel). In Fig. 2 we also note that an increased mass loss rate does not modify only the endpoint of the evolution, but also the entire track: blueward excursions appear when mass loss increases, and their extent is larger for higher mass loss rate (see the red, green, purple, and yellow tracks for the 15 $M_\odot$ star).

Using a similar approach, Renzo et al. (2017) performed a systematic study of the effects of mass loss

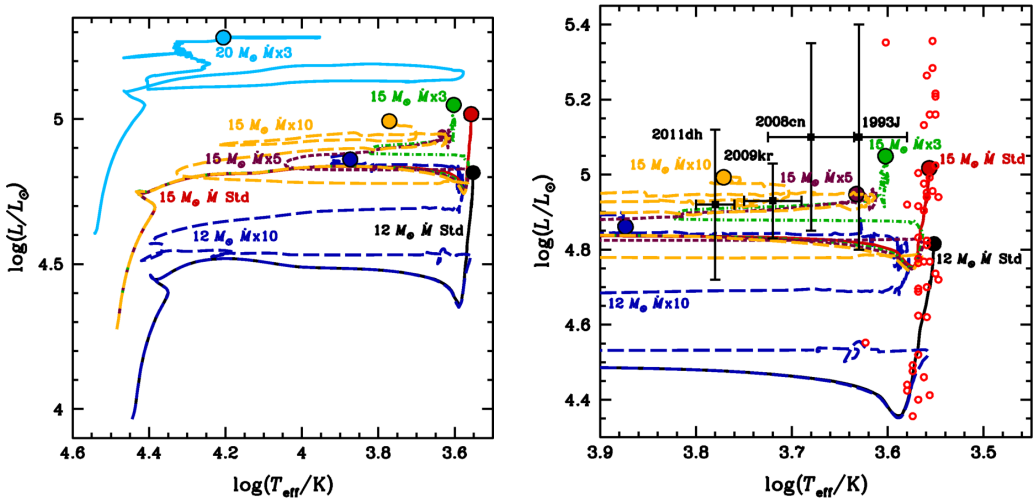


**Fig. 2.** Effect of mass loss in the RSG phase on the evolution of 12-20 $M_\odot$ stars. Mass loss multiplying factor are indicated on the tracks; Std refers to reference mass loss rate. The end point of the different evolutionary tracks are indicated by circles. The right panel is a zoom on the red/yellow supergiant region. Black squares indicate the position of progenitors of type II SN. The small red open circles are Galactic red supergiants. Figure from Georgy (2012).

prescriptions on the endpoints of evolutionary tracks (see also Sukhbold et al. 2018). They combined various mass loss recipes in the different phases of evolution (hot, cool and Wolf-Rayet phases). For each combination of mass loss recipes, they also introduced a scaling factor between 0.33 and 1.0 to take into account clumping effects. Their Fig. 9 shows the position of the endpoint of each evolutionary track. Stars with initial masses between 15 and 30 $M_\odot$ have endpoints that remain relatively stable. For instance the 15 $M_\odot$ track ends as a red or yellow supergiant (similar to Georgy 2012). Above 30 $M_\odot$ the endpoint is very sensitive to the mass loss prescriptions and CC SN progenitors can be Wolf-Rayet (WR), blue or yellow supergiants.

### *2.3 Metallicity*

The metal content has three main effects on the structure and evolution of massive stars. First, fewer metals implies smaller opacities, which translates into more compact stars with higher $T_{\rm eff}$. Second, due to the a higher compactness gradients are stronger in the star, which triggers the instabilities caused by rotation. Consequently in metal-poor stars the effects of rotation are strengthened. Third, mass loss rates in the hot phases (OB and WR stars) are driven by radiation pressure on metals. Hence, reduced metallicity implies reduced mass loss rates. The effects of metallicity on stellar evolution are thus multiple and intrinsically related to other processes.

Fig. 14 of Limongi & Chieffi (2018) show their evolutionary tracks that cover a wide range of initial masses, rotation rate and metallicities. In the right column (no rotation) we see that when metallicity decreases, tracks do not end any more in the hot part of the HR diagram: WR stars are not progenitors of supernovae and the most massive stars end their lives as blue supergiants, while the less massive ones explode as red/yellow supergiants. For models including rotation (middle and left columns) the general trend, compared to non-rotating models, is the displacement of the endpoints towards the blue/hot part of the HR diagram. WR stars can be progenitors of supernovae. However, the tracks ending their evolution in the blue part of the HR diagram have higher luminosities at low metallicity: a luminosity range [4.8-6.0] (in units of log $\frac{L}{L_\odot}$) is predicted at solar metallicity for stars ending their lives as WR, while this range is [6.0-6.7] at Z=1/1000 $Z_\odot$.

### *2.4 Binarity*

There are two main effects on the evolution of massive stars caused by the presence of a companion: the transfer of mass and angular momentum through Roche lobe overflow (RLOF), and the impact of tides on the internal structure and orbital parameters. The increased parameter space compared to single-star evolution makes it difficult to predict the general evolution of binary stars: in addition to the standard evolution of both stars, their interactions have to be taken into account. In practice, binary evolution codes have to make approximations.

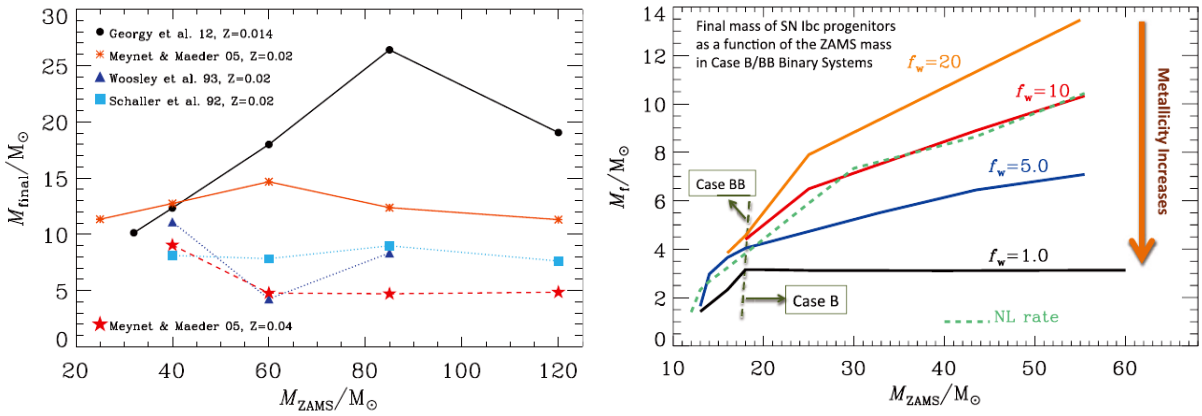


**Fig. 3.** Final mass as a function of initial mass for single (**left**) and binary (**right**) stars. Figure from Yoon (2015).

For instance, the BPASS binary models of Eldridge et al. (2017) do not include rotation and only follow in detail the evolution of the most massive component (prior to mass transfer).

Tidal forces imply an additional potential that needs to be taken into account to compute the internal structure and evolution. Angular momentum is transferred between the two components and the system's orbit, which is thought to lead to synchronization of the stars and orbital periods Zahn (1977). Mass transfer occurs when one of the components expands and fills its Roche lobe. Not only mass but also angular momentum is transferred. The efficiency of this process (fraction of the donor mass/angular momentum accreted by the companion) is one of the major uncertainties in binary evolution. The outcome of a binary interaction thus depends on a large number of parameters. See the reviews by Langer (2012) and Yoon (2015) for some insights.

## 3 Progenitors of type Ib/Ic supernovae

The search for progenitors of CC SN has so far been successful only for type II SN: there is only one tentative identification of a progenitor for each of the Ib and Ic categories. However, there are upper limits for several cases. Due to the absence of hydrogen in type Ibc SN, WR stars which have been stripped of their envelope by stellar winds are the natural candidates for such progenitors. As summarized by Smartt (2015), WN and WC stars in the Large Magellanic Clouds have R-band magnitudes between -7.0 and -2.0, while upper limits on the progenitors of type Ibc SN are in the range -7.0 to -4.0. There is thus a significant overlap and it is very unlikely that all progenitors that would have been a WN or WC stars were in the faint part of the distribution.

WO stars are the third type of WR stars. They are either a continuation of the WC sequence towards very high $T_{\rm eff}$, or a more evolved type of WR star that have experienced removal of a larger amount of external layers (see for instance Tramper et al. (2015)). Groh et al. (2014) have shown that a 60 $M_\odot$ star likely ended its life in this WO phase. The typical spectral energy distribution (SED) of such objects is compared to that of other progenitor candidates in the top panel Fig. 5 of Groh et al. (2013b). Because of the extremely high $T_{\rm eff}$, the WO SED is shifted towards the blue and in the usual optical and infrared filters, there is almost two orders of magnitude difference in the flux levels: WO stars are much fainter than WN or WC stars. If they are the progenitors of type Ibc supernovae, they are more difficult to detect. Fig. 10 and 11 of Groh et al. (2013b) predict that most endpoints of massive stars evolutionary tracks correspond to a WO star that is fainter than the upper limits on the magnitudes of type Ibc progenitors.

Single stars may thus lead to type Ibc SN, but binaries have been invoked for several reasons. The first argument is the mass of the SN ejecta - about 1 to 6 $M_\odot$ - which, combined to the mass of a neutron star, implies a progenitor mass lower than $\sim$8 $M_\odot$. Some single-star evolutionary calculations predict progenitor masses higher than this limit as illustrated in the left panel of Fig. 3. Binary star evolution may help to reduce these final masses due to the higher efficiency of mass removal by RLOF. The right panel of Fig. 3 shows that progenitor masses of the order 5-10 $M_\odot$ can be obtained for stars with initial masses in the range 20-60 $M_\odot$. Nonetheless, Fig. 3 highlights that the distinction between single and binary stars is not clear-cut since high-mass low metallicity binary progenitors and low-mass high-metallicity single star progenitors exist. In addition, the detection of stellar black holes with masses in excess of 10 $M_\odot$ (through gravitational waves detections) implies relatively high mass progenitors.

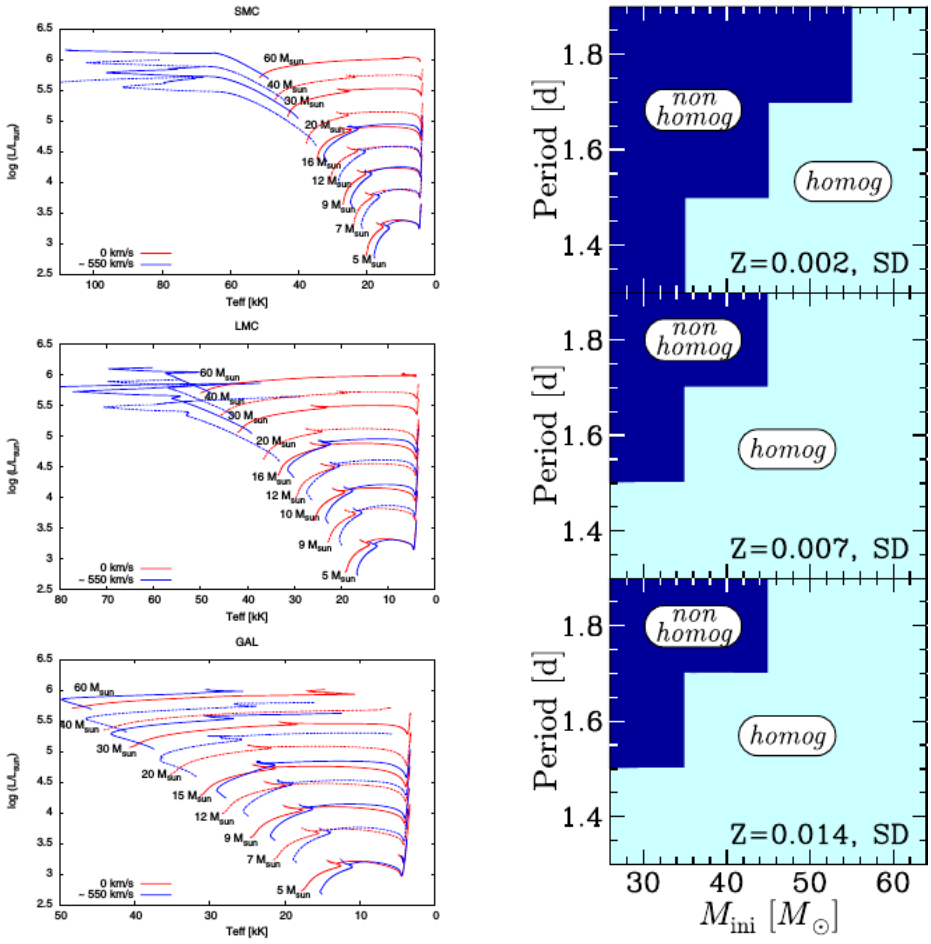


**Fig. 4. Left:** Evolutionary tracks of Brott et al. (2011) for three different metallicities (SMC, LMC and Galaxy, from top to bottom) and two rotational velocities (0 km/s in red and 550 km/s in blue). Figure from Brott et al. (2011). **Right:** Period as a function of initial mass in binary systems for three metallicities (Z=0.002, 0.07 and 0.014 from top to bottom). The cyan area corresponds to the parameter space where quasi homogeneous evolution takes place. From Song et al. (2016).

Binarity may also be invoked if one considers the number of type Ibc relative to type II SN. If the latter are caused by 8-20 $M_\odot$ stars, and the former by 20-100 $M_\odot$ stars, then assuming a Salpeter initial mass function, one would expect ∼15% of type Ibc SN, while we observe about 25%. Hence, at least part of the type Ibc SN may be due to stars with masses lower than 20 $M_\odot$. And for such stars to lose their hydrogen-rich envelope, mass transfer in a binary systems is more efficient than stellar winds which are weaker in this mass range.

## 4 Long-soft gamma-ray bursts and chemically homogeneous evolution

So far only broad-line type Ic SN have been associated with LGRBs. The current scenario for the production of LGRBs is the explosion of a very fast rotating star (collapsar model, Woosley et al. (1993)). The final collapse comes with the launch of a relativistic jet that peers through the outer layers of the progenitor, creating the high-energy emission. Fast rotation may partly explain the broad lines observed in the associated supernova.

Rotation affects the evolution and fate of massive stars (Sect. 2.1). So far we have only considered moderate rotation velocity (<40% of the critical velocity) while the collapsar model corresponds to near critical velocity. At such high rotation rates, the mixing timescale becomes shorter than the nuclear timescale and material produced by nucleosynthesis in the core is immediately redistributed throughout the entire star. There is no chemical gradient and the outer layers are chemically enriched. As a consequence, the opacity decreases, $T_{\rm eff}$ increases and the mean molecular weight increases. This leads to a blueward evolution in the HR diagram. This

type of evolution is called quasi chemically homogeneous evolution (CHE - Maeder 1987 and Langer 1992).

For a single star to rotate fast in the pre-supernova stage, there are two conditions: a high initial rotation and a limited loss angular momentum through stellar winds. In the course of CHE, the star remains in the blue part of the HR diagram where winds are radiatively driven. The associated mass loss rates depend on metallicity ($\dot{M} \propto Z^{0.8}$, see Mokiem et al. 2007). Hence angular momentum removal is weaker at lower metallicity and CHE is favoured. This is illustrated in the left column of Fig. 4. Fast rotation leads to the early blueward bifurcation of evolutionary tracks at metallicities of the Magellanic Clouds, but not at solar metallicity.

In binary stars very fast rotation is mainly observed after RLOF, when the receiver has been spun-up from the accretion of angular momentum. Stars being more compact at lower metallicity (see Sect. 2.3), RLOF is less frequent and occurs only in systems with the smallest separations. This is shown in the right column of Fig. 4. Hence CHE occurs preferentially at high metallicity in binary stars, in contrast to single stars.

Is there any observational evidence for CHE? Martins et al. (2009, 2013) have studied the properties of a few early WNh stars in the Magellanic Clouds and the Galaxy. These stars are located on the blue side of the zero age main sequence, where stars following CHE and normal WR stars are expected to be. The WNh stars studied by Martins et al. still have a significant hydrogen mass fraction in their envelope, contrary to normal WR stars that have lost their H-rich envelope. This is consistent with CHE.

## References


Brott, I., de Mink, S. E., Cantiello, M., et al. 2011, A&A, 530, A115

Cao, Y., Kasliwal, M. M., Arcavi, I., et al. 2013, ApJ, 775, L7

Chiosi, C. & Maeder, A. 1986, ARA&A, 24, 329

Ekström, S., Georgy, C., Eggenberger, P., et al. 2012, A&A, 537, A146

Eldridge, J. J., Stanway, E. R., Xiao, L., et al. 2017, PASA, 34, e058

Georgy, C. 2012, A&A, 538, L8

Groh, J. H. 2017, Philosophical Transactions of the Royal Society of London Series A, 375, 20170219

Groh, J. H., Georgy, C., & Ekström, S. 2013a, A&A, 558, L1

Groh, J. H., Meynet, G., Ekström, S., & Georgy, C. 2014, A&A, 564, A30

Groh, J. H., Meynet, G., Georgy, C., & Ekström, S. 2013b, A&A, 558, A131

Hirschi, R., Arnett, D., Cristini, A., et al. 2017, in IAU Symposium, Vol. 331, Supernova 1987A:30 years later - Cosmic Rays and Nuclei from Supernovae and their Aftermaths, ed. A. Marcowith, M. Renaud, G. Dubner, A. Ray, & A. Bykov, 1–10

Kippenhahn, R. & Weigert, A. 1994, Stellar Structure and Evolution, 192

Langer, N. 1992, A&A, 265, L17

Langer, N. 2012, ARA&A, 50, 107

Limongi, M. & Chieffi, A. 2018, ApJS, 237, 13

Maeder, A. 1987, A&A, 178, 159

Maeder, A. & Meynet, G. 2000, ARA&A, 38, 143

Martins, F., Depagne, E., Russeil, D., & Mahy, L. 2013, A&A, 554, A23

Martins, F., Hillier, D. J., Bouret, J. C., et al. 2009, A&A, 495, 257

Mauron, N. & Josselin, E. 2011, A&A, 526, A156

Meynet, G., Chomienne, V., Ekström, S., et al. 2015, A&A, 575, A60

Mokiem, M. R., de Koter, A., Vink, J. S., et al. 2007, A&A, 473, 603

Renzo, M., Ott, C. D., Shore, S. N., & de Mink, S. E. 2017, A&A, 603, A118

Smartt, S. J. 2009, ARA&A, 47, 63

Smartt, S. J. 2015, PASA, 32, e016

Song, H. F., Meynet, G., Maeder, A., Ekström, S., & Eggenberger, P. 2016, A&A, 585, A120

Sukhbold, T., Woosley, S. E., & Heger, A. 2018, ApJ, 860, 93

Tramper, F., Straal, S. M., Sanyal, D., et al. 2015, A&A, 581, A110

Van Dyk, S. D., Zheng, W., Brink, T. G., et al. 2018, ApJ, 860, 90

von Zeipel, H. 1924, MNRAS, 84, 665

Woosley, S. E., Langer, N., & Weaver, T. A. 1993, ApJ, 411, 823

Yoon, S.-C. 2015, PASA, 32, e015

Zahn, J.-P. 1977, A&A, 57, 383